Journal of Solid State Chemistry **154,** 214–222 (2000)
doi:10.1006/jssc.2000.8838, available online at http://www.idealibrary.com on IDEAL®

Boron Nitride Analogs of Fullerenes (the Fulborenes), Nanotubes, and Fullerites (the Fulborenites)

Vladimir V. Pokropivny,[1] Valery V. Skorokhod, Galina S. Oleinik, Alexander V. Kurdyumov, Tamara S. Bartnitskaya, Alex V. Pokropivny, Alexander G. Sisonyuk, and Dmitry M. Sheichenko

Institute for Problems of Materials Science, National Academy of Sciences of Ukraine, Krzhyzhanovsky str.3, Kiev 252142, Ukraine

Received September 9, 1999; in revised form February 10, 2000; accepted February 15, 2000

The molecules $B_{12}N_{12}$, $B_{24}N_{24}$ and $B_{60}N_{60}$ (named by us as fulborenes) have been proposed as boron nitride analogs of the fullerenes, especially $B_{60}N_{60}$ as the analog of C_{60}. Modified neglect of diatomic overlap computation was performed to confirm their stability. Multiwalled BN nanotubes and onions were produced by carbothermal synthesis. Their structure and mechanisms of growth and formation were studied by TEM, X-ray spectral microanalysis, and molecular dynamics techniques using B–B, B–N, and N–N original interatomic potentials. Ten possible zeolite-like crystals built from these molecules (named by us as fulborenites) were predicted, and their lattice parameters and densities were calculated. Comparison with explosive experiments allow us to identify the simple cubic fulborenite $B_{12}N_{12}$ with intermediate phase of BN. New original ideas were suggested of: (i) a "hyper-diamond" based on $B_{12}N_{12}$-fulborenite with zincblende lattice, (ii) a "superdense diamond" based on $Me_2B_{12}N_{12}$-fulborenide with bcc lattice, and (iii) a quantum hypersound generator based on BN nanotube.

Key Words: **boron nitride; fullerene; onion; nanotube; fullerite; fulleride; carbothermal synthesis.**

1. INTRODUCTION

Boron is known as a unique element in periodic table due to its natural ability to form cage molecules, clusters, and their skeleton lattices, such as B_{12}-icosahedron and tetragonal boron. The discovery of fullerenes by H. Kroto, R. Curl, and R. Smalley in 1985 (1) and carbon nanotubes by S. Iijima in 1991 (2) has given impetus to search for novel fullerene-like boron structures and their lattices, examples of which were presented at the 12th ISBB Symposium. For example, I. Boustsani has introduced new stable convex B_{16} and B_{46}, and spherical B_{22}, B_{32}, and B_{42} bare boron clusters (3–5), as well as an icosahedral $B_{12}H_{12}$ cluster simulating the B_{12} cluster in β-rhombohedral boron, have been investigated numerically (6). Due to similarity between graphite and graphene BN the recent discovery of novel fullerene-like nanostructures on the base of BN or other materials with layering structure was not a great surprise. Particularly, the $B_{30}N_{30}$ as a formal analog of buckminster-fullerene (7), the molecules $B_{12}N_{12}$, $B_{16}N_{16}$, $B_{36}N_{36}$ (8–11), the fullerene-like cages $B_{12+3n}N_{12+3n}$ (12), the BN, BC_3, and BNC nanotubes and polymers (13–20), the conjunctions of nanotubes (20), and the BN-heteroconnectors as quantum dots (21) were studied theoretically. Moreover the BN-onions (22,23) and nanotubes on the base of $B_xC_yN_z$ (24,25) and BN (26–32) were synthesized by different techniques, namely, by arc-discharge (24–28,31), laser (23,29), and carbothermal synthesis (22,30) and by the solid-state process (32). In addition to molecular crystals built from C_{60} molecules, the covalently bonded solids, such as C_{36} crystal (33), the polymers, such as C_{60} barrelenes (34), the clathrate-like Si_{46}, Si_{136}, GaAs, and other skeleton semiconductors (35,36), and the new zeolite-like BN crystals (37,38) were suggested. An increasing number of the fullerene materials is certain to open new research and technological avenues in the interface between chemical physics, solid-state physics, materials science, and nanotechnology at the beginning of 21 century.

In this work we describe our recent results in the prediction and modified neglect of diatomic overlap (MNDO) computations of the BN fullerene-like molecules (the fulborenes), the synthesis, experimental examination, and molecular dynamics simulation of BN-nanotubes (BN-NT), the prediction, and the preliminary experimental observation of zeolite-like BN crystals (the fulborenites).

2. FULBORENES

From the experimental standard formation enthalpy the energies of hybridized sp^2 and sp^3 B–N bonds are known to

[1] To whom correspondence should be addressed. E-mail: pokr@ipms.kiev.ua.

0022-4596/00 $35.00

be stronger in comparison with those B–B and N–N bonds, namely 4.00, 2.32, and 2.11 eV, respectively (39). Hence one can conclude rule 1 governing a formation of BN molecules (the fulborenes): the deviation from stoichiometric composition must be as small as possible. The EELS spectra taken from BN-nanotubes yield a B:N ratio of approximately 1 (27), giving credence to the rule. It is known that the isolated pentagons rule is adopted by a stability condition of the bukminsterfullerene C_{60} . It is a consequence of the more general rule 2: the conservation of valence 4 for three neighbors. These rules were used to search spherical BN-fulborenes among Archimed polyhedra, all atoms of which lie at a sphere. Three appropriate fulborenes fulfilling these rules are shown in Fig. 1 with their point symmetry groups, namely, T_h for $B_{12}N_{12}$, O for $B_{24}N_{24}$, and I for $B_{60}N_{60}$. Previously, only the $B_{12}N_{12}$ molecule was studied by *ab initio* calculations demonstrating its stability (8–12). Note that the molecules $B_{12}N_{12}$, $B_{24}N_{24}$, and $B_{60}N_{60}$ are the lowest of any other near-spherical molecules composed of 4-, 6-, 8-, and 10-membered rings, respectively.

The fulborenes were studied further by semiempirical and molecular dynamics techniques, both showing the thermodynamic stability of $B_{12}N_{12}$, $B_{24}N_{24}$, and $B_{60}N_{60}$ fulborenes.

Computations were performed by the semiempirical MNDO method developed by M. Dewar and W. Thiel (40) using both our original computer programs and the MOPAC package (41). All of the fulborenes were found to be stable in a processes of energy minimization in contrast to pure B_{24} molecule which was destroyed. Total energy of a molecule is the sum of the electronic energy and the repulsion between cores of atoms A and B, $E_{\text{tot}}^{\text{mol}} = E_{\text{el}} + \sum\sum_{A<B} E_{AB}^{\text{core}}$. Heat of formation was obtained from the total energy by subtracting the electronic energy and adding the experimental heats of formation of the atoms, $\Delta H_f^{\text{mol}} = E_{\text{tot}}^{\text{mol}} - \sum_A E_{\text{el}}^A + \sum_A \Delta H_f^A$. HOMO-LUMO band gap is the energy difference between a highest occupied molecular orbital (HOMO) level and a lowest unoccupied molecular orbital (LUMO) level. The calculated values of the fulborenes are presented in Table 1.

Like C_{60}, the $B_{60}N_{60}$ molecule derives from icosahedron by truncating its 12 apexes followed by further truncating 30 edge-connected pentagons. Just as C_{60}, the $B_{60}N_{60}$ have: (a) the icosahedron symmetry, (b) spherical form, or the lowest deviation of the sum of valent angles on 360°, $\sim 6°$ instead of $\sim 12°$ in C_{60} (c) 12 isolated decagons, 20 isolated hexagons, and 30 isolated tetragons instead of 12 isolated pentagons in C_{60}, (d) the lowest potential energy per atom (-5.63 eV/atom), which is evidence of its highest energetic stability, and (e) the highest HOMO-LUMO gap (8.73 eV) in comparison with other fulborenes which is a conventional sign of chemical stability. Hence, $B_{60}N_{60}$ is precisely the molecule of any known BN molecules, that we must recognize as an analog of buckminsterfullerene C_{60}.

Semiempirical calculation shows that 2 active vibration modes dominate in the infrared (IR) spectrum of $B_{12}N_{12}$ fulborene, namely, 1294 cm^{-1} and 825 cm^{-1} (the others have the relative intensity less than $\sim 10\%$), and 3 modes in the IR spectrum of $B_{24}N_{24}$ fulborene, namely, 1356 cm^{-1}, 1336 cm^{-1}, and 772 cm^{-1} (the others have the relative intensity less than 2.3%). Note that F. Yensen obtained 2 active IR modes, namely, 1649 cm^{-1} and 909 cm^{-1} for $B_{12}N_{12}$ fulborene by HF/STO-3G method (8). The peculiar frequencies of the breathing mode was calculated by us to be 722 cm^{-1} and 460 cm^{-1}, while the frequencies of squash or whispering mode was calculated to be 369 cm^{-1} and 217 cm^{-1} for $B_{12}N_{12}$ and $B_{24}N_{24}$ fulborenes respectively.

For MD simulations we have elaborated on the original interatomic potential for B–N system using the embedded-atom method developed by M. Daw and M. Baskes (42). Interatomic interaction in cage molecules, onions, and NTs is evident to be nearly the same as in graphene-like BN. Accounting of the short-range nature of covalent rigid bonding we considered the radius of interatomic interaction to be one of the main sensitive parameters determining the atomic rearrangement. It should be emphasized that usual

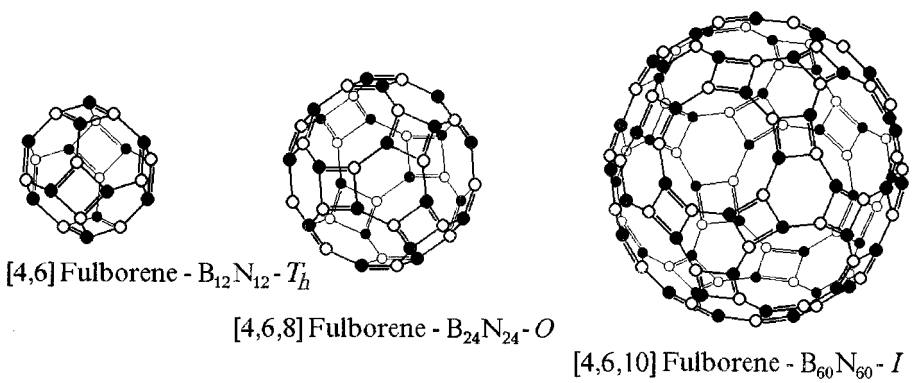

FIG. 1. Structure and symmetry (T_h, O, I) of fulborene molecules, in particular the $B_{60}N_{60}$ as an analog of buckminsterfullerene C_{60}.

TABLE 1
Parameters of the Fulborene Molecules

Fulborene	N_a	N_b	Tetragones	D_4 (nm)	Hexagones	D_6 (nm)	Octagones	Decagones	E_{tot}/N_a (eV)	ΔH_f^{mol} (eV)	Δ (eV)	q^*
$B_{12}N_{12}$	24	36	6	0.4089	8	0.3541			−5.13	−6.357	7.98	± 0.260
$B_{24}N_{24}$	48	72	12	0.6382	8	0.6045	6		−5.56	−8.098	8.34	± 0.311
$B_{60}N_{60}$	120	180	30	1.0804	20	1.0609		12	−5.63	−29.280	8.73	± 0.3

Note. N_a is the number of atoms, N_b is the number of bonds, D_4 and D_6 are the fulborene diameters along radial axes crossed tetragon and hexagon faces, respectively, E_{tot}/N_a is the total potential energy per atom, ΔH_f^{mol} is the heat of formation, Δ is the HOMO-LUMO gap, and q^* is the average charges per atom B (+) or N (−). The values in the last fourth columns were obtained by MNDO method with neighbor radius 7 Å.

Morse, Mee-Gruneisen, Buckingham, and other potentials converge very slowly, as seen in Fig. 2. Hence, a cutoff or smoothing procedure was used, but in either case artificial jumps in energy and/or force can arise during relaxation. To eliminate this problem the new special function was innovated, $\varphi(r) = A_k \cdot \ln^2[\rho(r)/\rho_0]/(r/r_k)^t - \varphi_0$, a peculiar feature of which is rapid convergence of itself and its derivative. This function automatically fulfills the equilibrium condition for cohesive energy $\varphi(r_0) = -\varphi_0$ and for lattice constant $\varphi'(r_0) = 0$, where φ' denotes a radius derivative. Electron density of s^2p^2 bonds $\rho(r) = 2R_{2s}^2(r) + 2R_{2p}^2(r)$ is expressed by parametrized wave functions for neutral N (or B) atoms $R_{2s} = A_1 \cdot r \cdot \exp(-\alpha_1 r) + A_2 \cdot \exp(-\alpha_2 r)$, $R_{2p} = A_1 \cdot r \cdot \exp(-\alpha_1 r)$. In addition the potential parameters fulfill the conditions for smooth end $\varphi(r_k) = \varphi'(r_k) = 0$. This type of potential may be considered as a Coulomb potential A_k/r^t screened by a functional of electron density $F[\rho(r)] = \ln^2[\rho(r)/\rho_0]$. Input data and obtained parameters for B–N potential are presented in Table 2. A plot of potentials with its derivative is shown in Fig. 2. In the same manner the potentials for B–B and N–N interactions were obtained, the input data, parameters, and plots of which are presented in Table 2 and Fig. 2, respectively. Note that equilibrium bond energy φ_0 for B–N, B–B, and N–N were found by H. Nozaki and S. Iton to reproduce correctly the relative stability of layered compounds BC_2N (39).

In recent time complex boride compounds have attracted much attention, such as BN–C–HfB_2/ZrB_2-based nanoparticles and nanotubes synthesized by A. Loiseau *et al.* in arc discharge (27,31), as well as the hard and tough eutectics alloys on the base of fibered LaB_6–$TiB_2/ZrB_2/HfB_2$ compounds synthesized by Yu. Paderno with coworkers using the directional cocrystallization technique (43). Theoretical description of this refractory boride meets the problem of describing chemical bonds between Me–B, B–B, and Me–Me atoms. The following questions arise: (i) what is the relative ratio of interaction forces between heterogeneous atoms, (ii) what is the level of intrinsic strain in compounds, (iii) how must the strain be characterized, and (iv) how is it dependent on structure and interatomic bonds. The set of self-consistent interatomic potentials for the

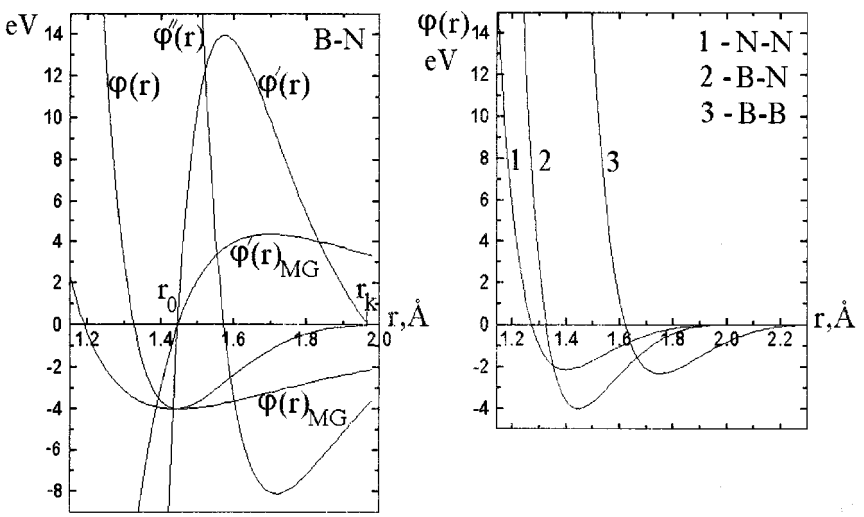

FIG. 2. Plots of our B–N potential with its derivative showing a well convergence in comparison with Mee–Gruneisen potential with its derivative marked as MG (left) and our B–N, B–B, and N–N potentials (right).

TABLE 2
Parameters of B–N, B–B, and N–N Interatomic Potentials $\varphi(r) = A_k \ln^2 [\rho(r)/\rho_0]/(r/r_k)^t - \varphi_0$

Bonds	r_0(Å)	φ_0 (eV)	r_k (Å)	A_k (eV)	t	A_1	α_1	A_2	α_2	ρ_0
B–N	1.4457	4.00	1.97	1.969865	7.975351	2s 6.2988 2p 6.1314	1.95	−8.1608	6.70	1.1484
B–B	1.75	2.32	2.30	2.990064	9.029879	2s 2.2747 2p 2.2250	1.30	−4.3335	4.70	0.6534
N–N	1.40	2.11	1.97	0.891192	7.385942	2s 6.2988 2p 6.1314	1.95	−8.1608	6.70	1.2868

Note. r_0 is the equilibrium distance, φ_0 is the depth of potential, r_k is the cutoff radius, A_k is the fitting parameter, ρ_0 is the equilibrium electron density, A_1, α_1, A_2, and α_2 are the exponent parameters for electron densities of atoms (see text). Note that φ_0 for B–B are very close for the heat of a rombohedral boron formation, ~550 kJ/mol, and r_0 for B–B is the equilibrium distance in TiB_2. For N–N the r_0 is equal to the double covalent radius of N.

above-mentioned compounds accounting recent achievements in design of potentials (44,45) was developed by us recently and will be reported elsewhere.

3. NANOTUBES

BN-onions and BN–NTs were synthesized by carbothermal reduction of ultradisperse amorphous boron oxide in the presence of nitrogen at 1100–1450°C by chemical reactions both in solid phase $B_2O_3 + 3B_4C + 7N_2 = 14BN + 3CO$ and in gas phase $B_2O_3 + 3CO + N_2 = 2BN + 3CO_2$ (30,38). Transmission electron microscopy (TEM) and X-ray microanalysis show several forms of the obtained multiwalled BN–NTs of 10–500 nm in diameter and of 1 nm–30 μm in length, including: (i) cylindrical NTs of the rectilinear, helical, smoothly curved or kinked forms and the concretions, triple junctions, etc. (Most of them terminate in a cap at one or both ends); (ii) NTs with a bamboo structure in the form of a succession of joined variable-diameter cylindrical NTs with caps or onions at the nodes (They often form NTs bundles and clusters); (iii) NTs in the form of a combination of truncated cones, one inserted into another. Some of the mentioned NTs are shown in Fig. 3. All types of NTs appear under the same conditions (temperature, nitrogen pressure). Often, the same NT contains fragments of NTs of different types, indicating a mechanism whereby one form of growth passes successively into another. X-ray microanalysis indicates the carbon-enriched segregation inside of the onions and bamboo nodes as seen from Fig. 3f.

Figure 4 shows the atomic structure of some single-walled BN–NTs. BN nanotubes are formed in both the gas and the solid phases (Fig. 3a).

Growth of NTs in vapor phase starts from a creation of growth centers at the surfaces of both onions and NTs during sticking of atoms and deposition of BN clusters, such as B_3N_3 and B_4N_4 rings, linear BN clusters, and so on (46). The structure and composition of these centers determine the internal structure of the tubes, such as an axis, chirality, and layering. NTs grow from onions by surface diffusion (47) and by incorporation of BN clusters at both open and closed ends. In the first case, the NTs grow as a continuation of onions by deposition on a prismatic plane of the (1120) or (1100) type, while in the second case the nucleus of NT is formed at a basal plane of onions surface. If the thickness of the walls changes gradually, the long NTs grow, and while the thickness increases rapidly, the NTs close. If the wall thickness increases, a convex cap with positive curvature in the growth direction forms at the end; when it decreases a concave cap forms. Such caps become centers of new NTs, whose growth is interrupted by the formation of onions too, and so on (Fig. 3e). Such a successive change in forms of growth (NT → onion → NT → onion) leads to formation of the bamboo structure (Figs. 3b and 3c). Growth of cylindrical tubes stops either when the free end is closed by onion or by sharp thinning of the wall in the growth direction. When growth occurs in the form of nested truncated cones, the thickness of the walls within one cone remains essentially unchanged, but the outer diameter decreases in the growth direction (Fig. 3d). For all forms of NTs, the outer diameter decreases characteristically in the growth direction.

BN–NTs with armchair configuration (Fig. 4a) grow preferentially to zigzag NTs (Figs. 4c and 4d) because the stability of BN clusters at the end is greater than that of BB or NN ones (48). In the first case the formation of tetragones traps the tip into a flat cap able to revert to a growing hexagonal network by incorporating incoming atoms, while in the second case the open–closed zigzag NT closes into an amorphous tip, preventing further growth (48).

The thickening and narrowing of multiwalled NTs are explained by the nonuniform growth of individual layers and formation of cylindrical terraces. As shown by molecular dynamic simulations, the formation of caps and cones of multilayer NTs is caused by formation of five (C_5, B_3N_2, etc.)- and seven (C_7, B_3N_4, etc.)- membered rings, leading to the thinning or thickening of growing NTs, respectively (49).

Growth of NTs in solid phase occurs during crystallization of the particles under cooling. A rising temperature

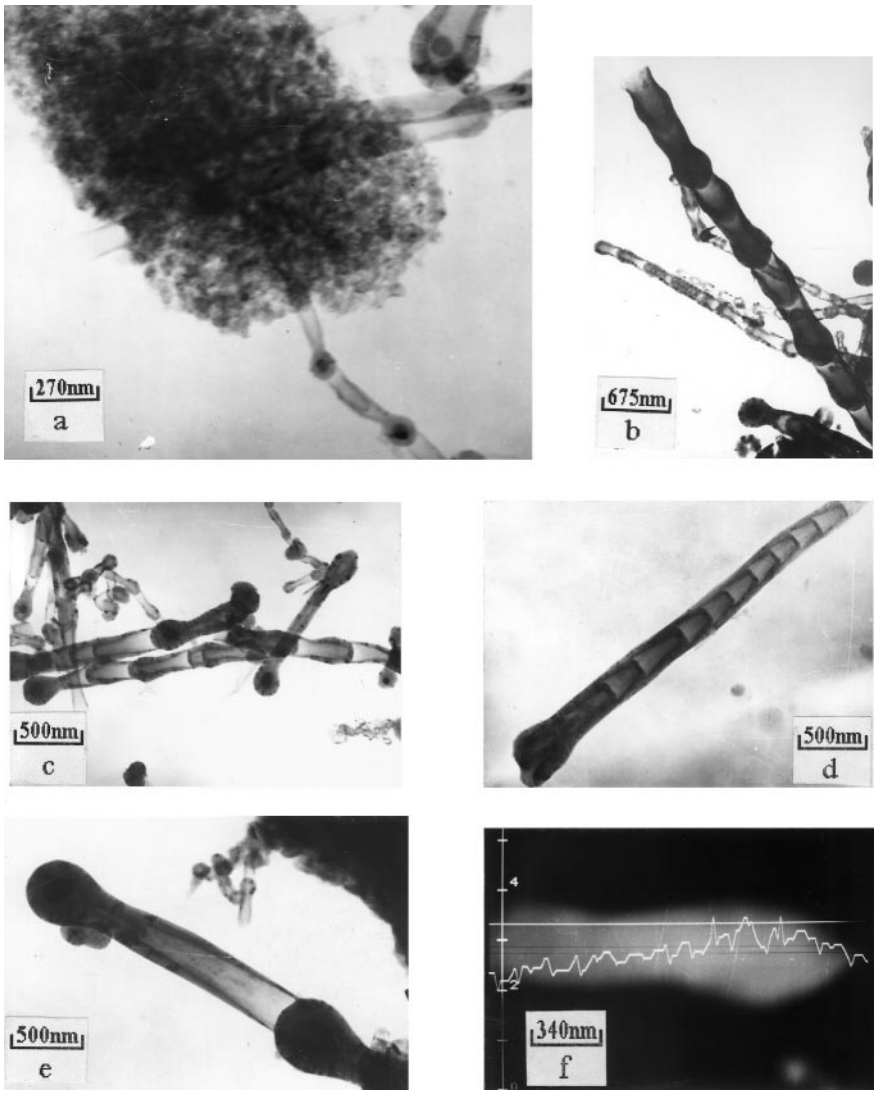

FIG. 3. Electron-microscope images of BN-NTs. (a) Growth in solid and gas phases; (b) bamboo NTs with open end; (c) bamboo NTs with closed-by-onion end; (d) NT in the form of nested truncated cones; (e) transformation of onion to cone-type NT; (f) electron probe microanalysis image of multiwalled NT together with X-ray microanalysis of carbon concentration profile (in relative units) along axis of NT closed-by-onion end, showing the carbon concentration increase at the onions.

gradient from the surface to the center of the particle is responsible for the decomposition of the solid BNC solution and precipitation of carbon inside the onion. TEM images show that such a carbon precipitates as beads or nodes in bamboo structure in Figs. 3b and 3c. Such a growth mechanism is in agreement with the Zang *et al.* (50) and Chen *et al.* (32) results.

Aimed at nanoelectronic application, the investigation of the electronic properties of NTs is a very active field of research now (see for example (19,21)). Also the elastic properties of C–NTs were studied experimentally (51,52) and simulated by the MD technique (17,53–55) aimed at exploring novel nanocomposite fibers and nanowires. N. Shopra and A. Zettl have estimated the Young's modulus of single-walled BN–NT by measuring oscillation amplitude, having an average value of 1.22 TPa (56). Due to the absence of interatomic potentials for BN systems only the tight-binding calculation of E.Hernandez *et al.* (17,57) was known for Young's modulus of single-walled BN–NT, $Y \simeq 0.88$ TPa. To calculate it by the MD method we also stretched both ends of NTs in opposite directions as shown in Fig. 4e. After every strain with small steps a full energy relaxation was performed using our interatomic potential. Also Young's modulus was calculated by summarizing second derivatives of all stretched ith bonds in a cross section of NT as $Y = 1/V\sum_{\mathrm{i}}(d^2\varphi_{\mathrm{i}}(r)/d\varepsilon^2)$, where V is a stretch volume. The estimated value was obtained to be

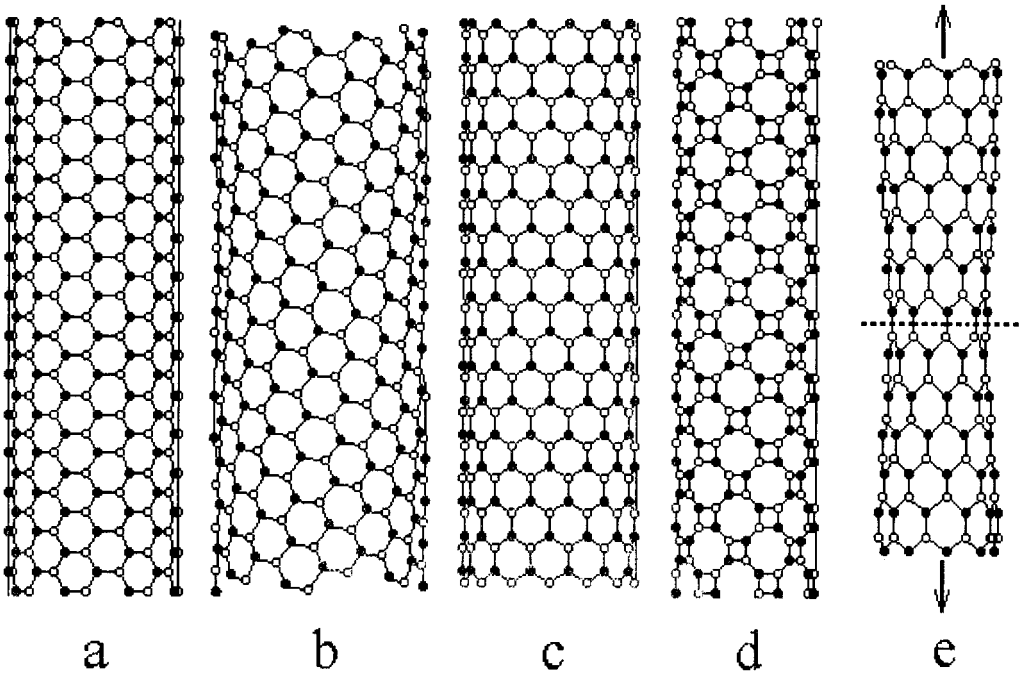

FIG. 4. Structure of single-walled BN nanotubes (N_a, number of atoms; N_b, number of interatomic bonds; θ, chiral angle; D, diameter; E_c/L, binding energy per unit length). (a) Armchair NT ($\theta = 30°$, $D = 1.10$ nm, $N_a = 640$, $N_b = 944$, $E_c/L = 17.1$ eV/nm; (b) chiral NT ($n = 7$, $m = 11$, $\theta = 22.7°$, $D = 1.253$ nm, $N_a = 653$, $N_b = 960$, $E_c/L = 10.7$ eV/nm; (c) zigzag NT ($\theta = 0°$, $D = 1.116$ nm, $N_a = 644$, $N_b = 952$, $E_c/L = 13.5$ eV/nm; (d) zigzag NT rolled from (3:4,8^2)-sheet ($D = 1.257$ nm, $N_a = 672$, $N_b = 994$, $E_c/L = 8.9$ eV/nm); (e) stretched NT under computation of Young's modulus, $Y \simeq 1.4$ TPa.

$Y \simeq 1.4$ TPa, close to the BN–graphene sheet one, showing slow dependence on NT diameter.

BN–NTs have to reveal unique properties, such as the predicted giant resonance effect (21), to make them suitable for new promising applications. For example, the whispering and breathing modes observed recently in Raman spectra from C–NTs (58) makes dielectric BN–NT without inversion center possible to use the as a quantum generator of hypersound or as phonon laser in the gigahertz–terahertz range.

In development of V. Ginzburg's conception of high-temperature superconductivity (59) a novel type of material was advanced by V. Pokropivny (60) as a perspective high-T_c superconductor based on its close-packed square or triangular lattice with $\simeq 2\lambda$ parameter (λ is a depth of field penetration) of quasi-1D superconducting nanotubes of

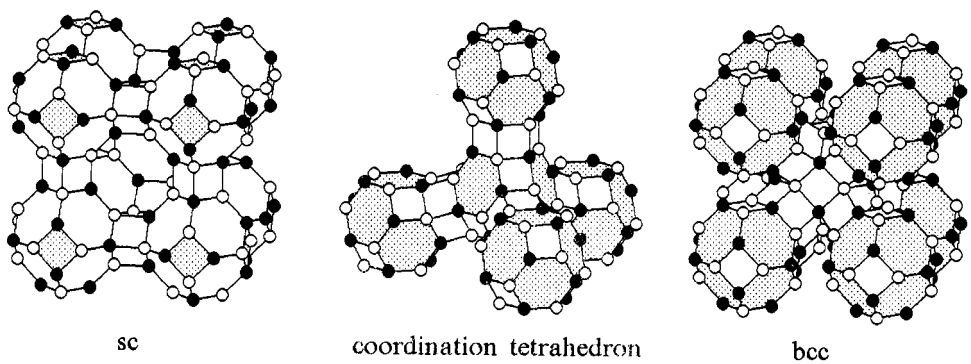

FIG. 5. Elementary unit cells of predicted $B_{12}N_{12}$ fulborenites with sc, simple cubic lattice; bcc, body- centered cubic lattice, the dopped analog of which, $Me_2B_{12}N_{12}$ or Me_2C_{24}, is referred to as a "superdense diamond"; and coordination tetrahedron, a building block of both a zincblende lattice (referred to as a "hyperdiamond") and a wurtzite lattice.

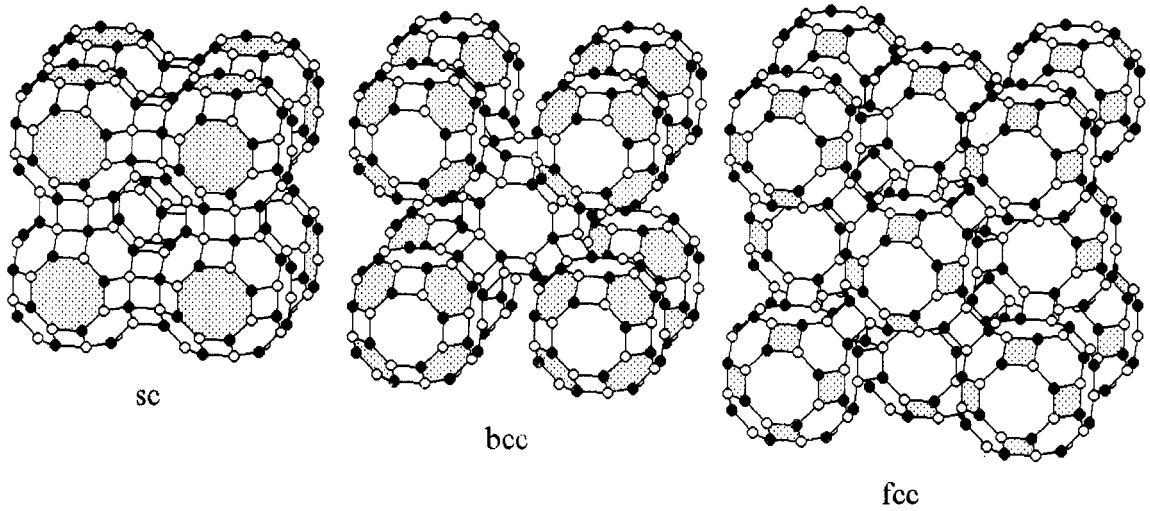

FIG. 6. Elementary unit cells of predicted $B_{24}N_{24}$ fulborenites with sc, simple cubic lattice; bcc, body-centered cubic lattice; and fcc, face-centered cubic lattice.

$\simeq \xi$ radius (ξ is a coherent length). The mechanism of supeconductivity has been proposed based on a whispering mode which was shown to be responsible for the strong enhancement of electron–phonon interaction and the increase of critical temperature. Such quasi-1D nanotubular crystal was proposed to be synthesized by a CVD template method using zeolite-like nanomembranes (60).

4. FULBORENITES

To outline all kinds of crystals that can be built from the fulborenes, one can suggest the simple crystallographic rules of symmetry: the coordination and type of molecular lattice are governed by a number and orientation of BN molecule faces (rule 3); and the number of covalent double bonds on both conjugated faces must be equal to a necessary number of intermolecular single bonds between two adjacent faces (rule 4).

According to the rules 3 and 4 the $B_{12}N_{12}$ molecules may be packed in the simple cubic (sc) lattice by conjugation of six tetragonal faces (Fig. 5). Conjunction of hexagonal faces according to rule 3 gives the body-centered cubic (bcc) lattice (Fig. 5) but with violation of rule 4 because only four of eight hexagons of $B_{12}N_{12}$ have the three necessary double bonds (Kekule structure). However, the angles between hexagons with double bonds are 109.47°, hence the coordination tetrahedron (Fig. 5) is permitted, creating a building unit of the the zincblende-type and wurtzite-type lattice instead of bcc lattice. Such a giant diamond-type crystal built from $B_{12}N_{12}$ molecules we refer to here as a "hyperdiamond."

Bcc-fulborenite $B_{12}N_{12}$ as well as bcc-fullerite C_{24}, if synthesized, looks very tempting because their densities are

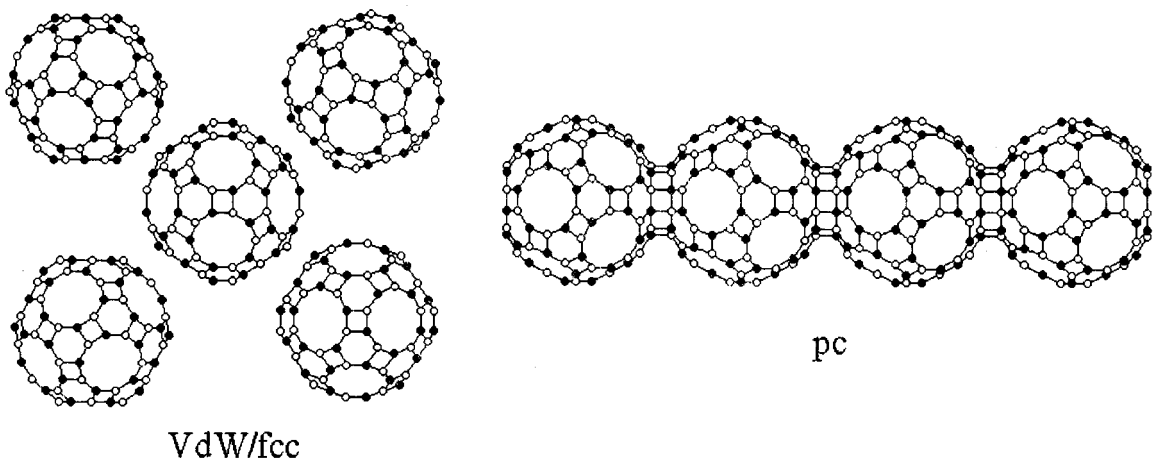

FIG. 7. Elementary unit cell of Van der Waals fcc fulborenites (VdW/fcc) and inorganic polymeric chain (pc) consisted of $B_{60}N_{60}$ molecules.

TABLE 3
Lattice Parameters (a and c) and Densities of Suggested Fulborenites

No	Molecule	Lattice	a (Å)	c (Å)	d (g/cm^3)
1	$B_{12}N_{12}$	sc	5.535–5.991	—	2.917–2.299
2		bcc	5.758–6.234	—	5.180–4.083
3		Zincblende	11.517–12.467	—	2.590–2.042
4		Wurtzite	8.144–8.816	13.298–14.396	2.243–1.718
5		VdW/fcc	11.175	—	1.417
6	$B_{24}N_{24}$	sc	6.980–7.556	—	2.908–2.292
7		bcc	8.650–9.364	—	3.057–2.410
8		fcc	11.069–11.983	—	2.917–2.299
9		VdW/fcc	14.1870	—	1.385
10	$B_{60}N_{60}$	VdW/fcc	20.2609	—	1.189

Note. The lower and upper limits correspond to the length of graphite-like (1.4457 Å) and diamond-like (1.565 Å) bonds, respectively. VdW/fcc is the fcc-lattice with Van-der-Waals intermolecular bonds of 3.3306 Å length, which is equal to the interlayer distance in graphite-like BN.

grater than for cubic BN and diamond respectively by a factor of 1.5. Unfortunately their formation is impossible due to the lack of necessary intermolecular bonds between adjacent hexagonal faces. However, these faces may be assumed to be bounded by some interstitial impurities inserted in small octahedral voids between molecules at the $\langle 100 \rangle$ edges of bcc-lattice. In this way, one may obtain the exohedral fullerides such as $Me_2B_{12}N_{12}$ or Me_2C_{24}, where Me is a light electron donor element, for example, Li, Be, etc. We refer to them here as "superdense diamonds."

The $B_{24}N_{24}$ molecules may be packed in three lattices, namely, the sc-lattice by conjugation of 6 octagonal faces, the bcc-lattice by conjugation of 8 hexagonal faces, and the face-centered cubic (fcc) lattice by conjugation of 12 tetragonal faces (Fig. 6).

The $B_{60}N_{60}$ molecules satisfy neither rule 3 nor rule 4 and therefore any close-packed lattices are impossible. However, there are no restrictions to creating Van der Waals molecular crystals as well as inorganic polymeric chains, some of which are shown in Fig. 7.

Calculated parameters of these 10 predicted lattices are presented in Table 3 (37,38). Note that a great number of molecular crystals and polymeric chains can be built from all of the above molecules.

Some shock wave treatment data provide support for the crystals with many atoms per unit cell and density which is intermediate between graphite-like BN and zincblende-like BN (61–64). A. Kurdyumov and A. Pilyankevich in some explosive specimens (61) have observed the new intermediate phase with lattice parameter of cubic unit cell $a = 5.65$ Å involved 24 atoms and with density $d = 2.76$ g/cm^3. This is in close agreement with the parameters of sc-fulborenites $B_{12}N_{12}$ shown in Fig. 5 and Table 3. However, there is no good accordance with the structure of intermediate E-phase obtained in explosive experiments by T. Akashi *et al.* (62) and S. Batsanov (63,64). In our opinion this discrepancy arises from the intermediate BN phases diversity.

New skeleton-like BN phases predicted here are expected to have unique properties and promising applications. For example, the molecule relative rotation, suggested to form sc-$B_{12}N_{12}$, zincblende-$B_{12}N_{12}$ and bcc-$B_{24}N_{24}$ crystals, leads one to predict Davydov splitting of absorption optic spectra in such fulborenites. Like zeolites, the fulborenites with sc-lattices contain nanoporous channels of molecular dimensions that together with a rigid crystalline network, make them very attractive as molecular sieves and nanomembranes. Also, encapsulated fulborenites (fulborenides) could give rise to an abundance of novel nanocomposite materials.

1. Novel routes for synthesis of BN and BCN NTs were reported, namely, the substitution reaction technique by W. Han *et al.* (65, 66), when carbon atoms are substituted by B and N atoms without topological changes, and the pyrolysis method by R. Sen *et al.* (67).

2. Experimental evidence for creation of the nearly spherical single-shelled BN fullerene and the rectangle-like 4-shelled fulborene under electron irradiation of cubic or turbostratic BN was presented by O. Stephan *et al.* (68), and D. Golberg *et al.* (69). The model of this 4-shelled BN onion was proposed, namely, $B_{12}N_{12}@B_{76}N_{76}@B_{208}N_{208}@B_{412}N_{412}$ (68). Diameter (0.9 nm–1.0 nm) and shape of the single-shelled BN fullerene shown on HRTEM image in Fig. 2 of Ref. (69) is close to both the diameter (1.06 nm–1.08 nm in Table 1) and shape of $B_{60}N_{60}$ fulborene after energy optimization, that may be considered as the existence of $B_{60}N_{60}$. Furthermore a difference between the radius of $B_{12}N_{12}$ and $B_{60}N_{60}$ molecules (0.336 nm in Table 1) is very close to an interlayer distance in hexagonal BN (0.333 nm), allowing us to suggest the $B_{60}N_{60}$ fulborene as the second shell of the 4-shelled onion instead of $B_{76}N_{76}$ molecule.

3. Pentagonal and heptagonal BN rings were found in cups of BN NTs (70) which are energetically less favorable compared with the 4-, 6-, 8-, and 10-rings of the fulborenes. It was concluded that kinetics rather than thermodynamics dominate the growth of BN nanotubes because there is not sufficient time for annealing-out of such growth defects (71). Hence one can suggest the great population of BN fulborenes, onions, cups and nanostructures to be synthesized depending of the process parameters.

REFERENCES

1. H. W. Kroto, J. R. Heath, S. C. O'Brien, R. F. Curl, and R. E. Smalley, *Nature* **318,** 162 (1985).
2. S. Iijima, *J. Microsc.* **119,** 99 (1980); *Nature* **354,** 56 (1991).
3. I. Boustani, *J. Solid State Chem.* **133,** 182 (1997).
4. I. Boustani, A. Rubio, and J. A. Alonco, *Chem. Phys. Lett.* **311,** 21 (1999).
5. I. Boustani, A. Quandt, E. Hernandez, and A. Rubio, *J. Chem. Phys.* **110,** 3176 (1999).
6. M. Fujimori and K. Kimura. *J. Solid State Chem.* **133,** 178 (1997).
7. X. Xia, D. A. Jelski, J. R. Bowser, and T. F. George, *J. Am. Chem. Soc.* **114,** 6493 (1992).
8. F. Jensen and H. Toftlund, *Chem. Phys. Lett.* **201,** 89 (1993).
9. I. V. Stankevich, A. L. Chistyakov, and E. G. Galpern, *Izv. Acad. Nauk. Ser. Khim.* (*Russ. Chem. Bull.*) **10,** 1712 (1993).
10. I. V. Stankevich, A. L. Chistyakov, E. G. Galpern, and N. P. Gambaryan, *Zh. Struct. Khim.* **36,** 976 (1995).
11. S. S. Alexandre, M. S. Mazzoni, H. Chacham, *Appl. Phys. Lett.* **75,** 61 (1999).

12. I. S. Dumitrescu, F. L. Ochoa, P. Bishof, and I. Haiduc, *J. Mol. Struct.* (*Theochem.*) **367,** 47 (1996).
13. A. Rubio, J. L. Corcill, and M. L. Cohen, *Phys. Rev. B* **49,** 5081 (1994).
14. X. Blase, A. Rubio, S. G. Louie, and M. L. Cohen, *Europhys. Lett.* **28,** 335 (1994).
15. Y. Miyamoto, A. Rubio, M. L. Cohen, and S. G. Louie, *Phys. Rev. B* **50,** 4976 (1994); 18360 (1994).
16. H.-Y. Zhu, G. J. Klein, W. A. Seitz, and N. H. March, *Inorg. Chem.* **34,** 1377 (1995).
17. E. Hernandez, C. Goze, P. Bernier, and A. Rubio, *Appl. Phys. A* **68,** 287 (1999).
18. X. Blase, J.-Ch. Charlier, A. De Vita, and R. Car, *Appl. Phys. Lett.* **70,** 197 (1997).
19. X. Blase, J.-Ch. Charlier, A. De Vita, and R. Car, *Appl. Phys. A* **68,** 267, 293 (1999).
20. Ph. Lambin and V. Meunier, *Appl. Phys. A* **68,** 263 (1999).
21. L. A. Chernozatonskii, Ya. K. Shimkus, and I. V. Stankevich, *Phys. Lett. A* **240,** 105 (1998).
22. T. S. Bartnitskaya, T. Ya. Kosolapova, A. V. Kurdyumov, G. S. Oleinik, and A. N. Pilyankevich, *J. Less-Common Met.* **117,** 253 (1986).
23. L. Boulanger, B. Andriot, M. Cauchetier, and F. Willaime, *Chem. Phys. Lett.* **234,** 227 (1995).
24. O. Stephan, P. M. Ajayan, C. Colliex *et al.*, *Science* **266,** 1683 (1994).
25. Z. Weng-Sieh, K. Cherrey, N. G. Chopra, X. Blase, Y. Miyamoto, A. Rubio, M. L. Cohen, S. G. Louie, A. Zettl, and R. Gronsky, *Phys. Rev. B* **51,** 11229 (1995).
26. N. G. Chopra, R. L. Luyken, K. Cherrey, V. H. Crespi, M. L. Cohen, S. G. Louie, and A. Zettl, *Science* **269,** 966 (1995).
27. A. Loiseau, F. Willaime, N. Demoncy, G. Hug, and H. Pascard, *Phys. Rev. Lett.* **76,** 4737 (1996).
28. K. Suenaga, C. Colliex, N. Demoncy, A. Loiseau *et al.*, *Science* **278,** 653 (1997).
29. D. Golberg, Y. Bando, M. Eremets, K. Takemura, K. Kurashima, and H. Yusa, *Appl. Phys. Lett.* **69,** 2045 (1996).
30. T. S. Bartnitskaya, G. S. Oleinik, A. V. Pokropivny, and V. V. Pokropivny, *JETP Lett.* **69,** 163 (1999).
31. K. Suenaga, F. Willaime, A. Loiseau, and C. Colliex, *Appl. Phys. A* **68,** 301 (1999).
32. Y. Chen, L. T. Chadderton, J. F. Gerald, and J. S. Williams, *Appl. Phys. Lett.* **74,** 2960 (1999).
33. C. Piscoti, J. Yarger, and A. Zettl, *Nature* **393,** 771 (1998).
34. L. A. Chernozatonskii, E. G. Galpern, and I. V. Stankevich, *Pis'ma ZhETP* **67,** 678 (1998).
35. A. A. Demkov, W. Windl, and O. F. Sankey, *Phys. Rev. B* **53,** 11288 (1997).
36. A. A. Demkov, O. F. Sankey, J. Gryko, and P. F. McMillan, *Phys. Rev. B* **55,** 6904 (1997).
37. V. V. Pokropivny, A. V. Pokropivny, V. V. Skorokhod, and A. V. Kurdyumov, *Dopov. Akad. Nauk Ukr.* (*Proc. Natl. Acad. Sci. Ukraine*) **4,** 112 (1999).
38. V. V. Pokropivny, V. V. Skorokhod, A. V. Kurdyumov, G. S. Oleinik, T. S. Bartnitskaya, and A. V. Pokropivny, *Proc. of SPIE's* 44. "Eng. Nanostructural Films and Materials" (A. Lakhtakia and R. F. Messier, Ed.) Vol. 3790, 213 (1999).
39. H. Nozaki and S. Itoh. *J. Phys. Chem. Solids* **57,** 41 (1996).
40. M. J. Dewar and W. Thiel, *J. Am. Chem. Soc.* **99,** 4899, 4907 (1997).
41. J. J. Stewart, *MOPAC/7 Manual* 1993.
42. M. S. Daw and M. I. Baskes, *Phys. Rev. B* **29,** 6443 (1984).
43. Yu. B. Paderno *in* "Advanced Multilayered and Fibre-Reinforced Composites" (Y. M. Haddad, Ed.), pp. 353. Kluwer Academic, Dordrecht, 1998.
44. V. V. Ogorodnikov and Yu. I. Rogovoi, *Fiz. Tekh. Vys. Davlenii*, **1,** 43 (1994). [in Russian]
45. V. V. Pokropivny, V. V. Ogorodnikov, *Inorg. Mater.* **32,** 321 (1996). [in Russian]
46. J. M. Martin, J. El-Yazal, J. P. Francois, and R. Gijbels, *Chem. Phys. Lett.* **232,** 289 (1995).
47. O. A. Louchev, *Appl. Phys. Lett.* **71,** 3522 (1997).
48. X. Blase, A. De Vita, J. C. Charlier, and R. Car, *Phys. Rev. Lett.* **80,** 1666 (1998).
49. C. J. Brabec, F. Maiti, C. Roland, and J. Bernholc, *Chem. Phys. Lett.* **236,** 150 (1995).
50. X. F. Zang, X. B. Zang, G. Van Tendello *et al.*, *J. Crystal Growth* **130,** 368 (1994).
51. M. M. Treacy, T. W. Ebbsen, and J. M. Gibson, *Nature* **381,** 678 (1996).
52. S. Iijima, C. Brabec, A. Maiti, and J. Bernholc. *J. Chem. Phys.* **104,** 2089 (1996).
53. B. I. Yacobson, C. J. Brabec, and J. Bernholc. *Phys. Rev. Lett.* **76,** 2511 (1996).
54. J. P. Lu. *Phys. Rev. Lett.* **79,** 1297 (1997).
55. T. Halicioglu, *Thin Solid Films* **312,** 11 (1998).
56. N. G. Chopra, A. Zettl, *Solid State Commun.* **105,** 297 (1998).
57. E. Hernandez, C. Goze, P. Bernier, and A. Rubio, *Phys. Rev. Lett.* **80,** 4502 (1998).
58. A. M. Rao, E. Richter, S. Bandow *et al.*, *Science* **275,** 187 (1997).
59. V. L. Ginzburg, *Usp. Fiz. Nauk* **167,** 429 (1997).
60. V. V. Pokropivny, *J. Superconduct.* **13,** 607 (2000); *Metallofizika Noveishie Tekh.* **22,** (2000) (in press).
61. A. V. Kurdyumov and A. N. Pilyankevich, *in* "Bor. Sintez, structura i svoistva," p. 181. Nauka, Moscow, 1974.
62. T. Akashi, H. R. Pak, and A. B. Sawaoka, *J. Mater. Sci.* **21,** 4060 (1986).
63. S. S. Batsanov, L. J. Kopaneva, and E. V. Lazareva, *Propellants, Explos. Pyrotech.* **18,** 352 (1993).
64. S. S. Batsanov, *Fiz. Goreniya Vzryva* **34,** 117 (1998). [in Russian]
65. W. Han, Y. Bando, K. Kurashima, and T. Sato, *Chem. Phys. Lett.* **299,** 368 (1999).
66. D. Golberg, Y. Bando, W. Han, K. Kurashima, and T. Sato, *Chem. Phys. Lett.* **308,** 337 (1999).
67. R. Sen, B. C. Satishkumar, and A. Govindaray *et al.*, *Chem. Phys. Lett.* **287,** 671 (1998).
68. O. Stephan, Y. Bando, and A. Loiseau *et al.*, *Appl. Phys. A* **67,** 107 (1998).
69. D. Golberg, Y. Bando, O. Stephan, and K. Kurashima, *Appl. Phys. Lett.* **73,** 2441 (1998).
70. Y. Saito, M. Maida, and T. Matsumoto, *Jpn. J. Appl. Phys. Pt. 1A* **38,** 159 (1999).
71. D. Golberg, Y. Bando, M. Eremets *et al.*, *Chem. Phys. Lett.* **279,** 191 (1997).